NUMERICAL SIMULATION RESEARCH ON EFFICIENT DUST CAPTURE OF BLAST FURNACE TAP HOLE

Lili WANG[1], Wei WANG[2], Ran LI[3,*], Guangkuo HE[4], Haibin KE[5]

The traditional fixed dust collection hoods for blast furnace tap holes rely solely on passive negative pressure for dust capture, with limited suction capacity. The on-site dust removal efficiency is only 60%~70%. The overflowing dust seriously endangers workers' health and pollutes environment. This article designs a top rotating blade type composite dust collection hood and uses numerical simulation to systematically study the effects of rotation domain diameter, blade number, rotation speed on flow field structure, particle motion trajectory, and capture efficiency, and reveals the mechanism of vortex enhanced dust collection. The results showed that the optimal structure and operating parameters are a rotation domain diameter of 1.5 m, 6 blades, and a rotation speed of 3000 r/min, achieving a dust collection efficiency of 94%. This study provides a reliable theoretical basis and practical reference for the technical upgrading of dust removal equipment at blast furnace tap holes and promotes green production in blast furnace operations.

Keywords: Blast furnaces tap hole; a top rotating blade type composite dust collection hood; airflow distribution; dust capture; numerical simulation.

1. Introduction

The carbon emissions of steel industry account for more than 15% of the national industrial carbon emissions [1]. Blast furnace iron-making is an important part of steel production, emitting a large amount of dust during iron tapping process. On average, each ton of pig iron releases 2.5 kilograms of dust, and a large blast furnace produces approximately 25 tons of dust daily. When opening and blocking a blast furnace tap hole, initial jet velocity is 25 m/s, temperature is 1000℃, fine particulate dust(<10μm) accounts for up to 95%, and

[1] Associate Professor., Hebei Key Laboratory of Intelligence Equipment Digitalize Design and Process Simulation, Tangshan University, Tangshan, China, e-mail: 13703253408@163.com
[2] Lecturer., School of Mechanical and Electrical Engineering, Tangshan University, Tangshan, China, e-mail: 183658517@qq.com
[3*] Lecturer., School of Mechanical and Electrical Engineering, Tangshan University, Tangshan, China, e-mail: 469273590@qq.com
[4] Bachelor., School of Mechanical and Electrical Engineering, Tangshan University, Tangshan, China, e-mail: 3337976767@qq.com
[5] Senior Engineer., Ironmaking Plant, HBIS Group Tangsteel Company, Tangshan, China, e-mail: kehaibin928@126.com

exhibits the characteristic of intense instantaneous outburst [2], capture efficiency of traditional fixed dust collection hood is only 60-70%[3,4]. The overflowing dust not only threats workers' health but also pollutes environment [5,6]. Simultaneously, a large amount of dust is emitted directly also means that valuable iron-containing (TFe≈50%) dust resources are wasted. This is inconsistent with the current requirements of cost reduction, efficiency improvement, green and sustainable development in steel industry [7]. Therefore, the unorganized emission of dust from the blast furnace iron-making process is a key control target for air pollution in the steel industry, efficient capture and purification of dust during iron tapping process have become one of the key tasks for steel enterprises to achieve clean production, fulfill environmental protection responsibilities, and ensure production safety.

There were relevant studies on the design and application of dust collection hoods both domestically and internationally. Chi [8] addressed the difficulty in collecting dust from upper part of blast furnace raw material bins to perform reciprocating dust collection by utilizing mobile ventilation ports, effectively controlling dust pollution. Wu [9] utilized negative pressure to capture smoke dust during the renovation of the electric furnace dust collection system. Robert [10] designed a dust collection device for small melting furnaces, structurally optimizing to reduce dust dispersion. As a vital component of entire dust collection device, dust collection hood directly determines dust collection efficiency. However, actual measurements are often laborious, costly, and difficult to accurately obtain dust distribution. Currently, most scholars use CFD-DEM numerical simulations to study gas motion and particle distribution in gas-solid two-phase flow [11]. Wang [12] simulated the diffusion of blast furnaces multiple dust sources based on the k-ε model and confirmed that for every 0.1 m reduction in the distance between hood and dust source, the efficiency increased by 3%-5%. Lv[13] used Fluent fluid software to calculate dust collection efficiency of coal conveyor belt dust collection hood. And found that opening angle of dust collection hood had a significant impact on it. Geng [14] analyzed spatial distribution of dust movement in a steel-making electric furnace workshop through numerical simulation, and improved dust removal efficiency to 84% by optimizing structure of dust hood.

Blast furnaces tap hole dust removal is a challenging task. The negative pressure at the top of the traditional dust collection hood is only -200 Pa, and passive suction is difficult to match the transient strong jet of tap hole. Designing an efficient dust removal hood is an effective solution. Existing research mainly focuses on fixed static hoods, which have insufficient adaptability to dynamic jet and transient high concentration working conditions at tap holes. This study introduces the active disturbance of rotating blades into the dust removal of blast furnace tap holes for the first time. The SST k-ω+DPM high-precision coupling model is used to quantify the influence mechanism of structure and operating parameters on the capture effect, filling the research gap in the application of dynamic dust removal in blast furnace tap holes. Each unit is projected to reduce annual dust emissions by 320 tons, this meets the effective control of dust emission, which is a great significance for ensuring safe production and workers' occupational health.

2. Materials and methods

2.1 Background of Dust Collection Hood Design

A dust collection hood is installed above the tap hole area which is sealed with an integrated cover. The dust collection hood is connected to the purification equipment through a pipeline. Traditional dust collection hoods rely on negative pressure provided by a centrifugal fan in the iron-making workshop to capture dust, the negative pressure is -200Pa at top of traditional dust collection hood. The captured dust gas flows through a pipeline to purification device, where the dust is collected. The purified gas is discharged through a chimney, completing the entire dust removal process, which is shown in Figure1.

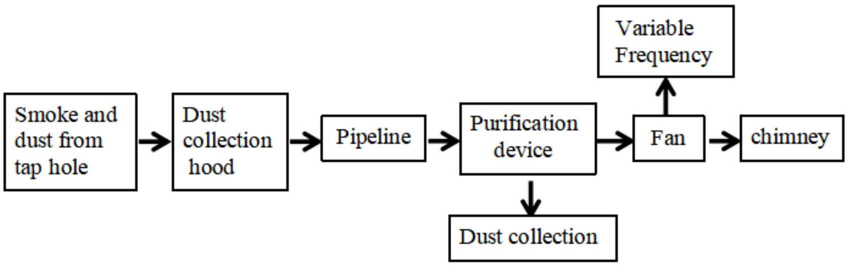

Fig. 1. Flow chart of the entire dust removal process

Dust collection hood is the first step in dust removal process, and it directly affects processing load of subsequent purification equipment and operational efficiency of overall dust removal system. The traditional dust collection hood is a fixed negative pressure exhaust hood, which relies solely on negative pressure passive exhaust to form weak airflow with velocity of <5 m/s. The stagnant flow field is large and the suction distribution is uneven. The jet instantaneous velocity is 25 m/s, far exceeding the suction capacity of the hood. The dust emission concentration can reach 5-8g/m^3, which cannot meet the requirement of dust concentration ≤15mg/m^3 in GB 28662-2012 "Emission Standards for Air Pollutants in the Iron and Steel Industry". Current situation of dust emission is shown in Figure 2.

Fig. 2. Current situation of dust emission

2.2 Dust Collection Hood Design

To solve this problem, this paper proposes a composite structure of "fixed hood body + rotation blades" based on traditional dust collection hood, as shown in Figure 3. Rotating shaft of rotation blades assembly coincides with the central axis of dust collection hood, and is perpendicular to gas inlet direction. Rotation generates forced vortices and active suction, which superimposes with the original negative pressure to form a strong disturbance, high-speed, and fully covered flow field. This active airflow disturbance structure has stronger dust guidance and control capabilities. This is in sharp contrast to the traditional dust collection hood that lacks dynamic structure.

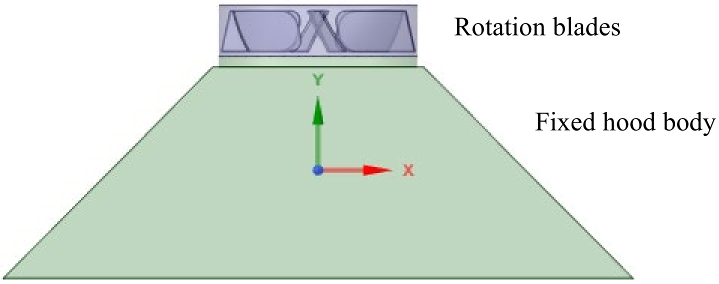

Fig.3. Dust collection hood

2.3 Chemical composition and particle size distribution of dust

Average dust production rate is 168kg/h. Chemical composition of dust is assayed by X-ray fluorescence spectroscopy(ZSX Primus IV from Nippon Rikyu), as shown in Table1. Particle size distribution is measured by laser diffraction particle size analyzer(Mastersizer 3000), as shown in Table 2.

Table 1

The chemical composition of dust

Composition	Fe_2O_3	FeO	TFe	CaO	MgO	SiO_2	P	Ash
Ratio(%)	59.76	9.12	48.9	5.38	0.3	5.06	0.013	13.84

Table 2

The particle size distribution of dust

Diameter(μm)	<1	1-3	3-5	5-10	>10
Ratio(%)	16	29	27	23.5	4.5

From Table 1, the main chemical component of dust is iron oxide. Therefore, the parameters of dust are considered as those of iron oxide, with a density of 4580 kg/m^3. From Table 2, dust diameters are very small with 95.5% less than 10μm, which can be inhaled into the respiratory tract, posing serious hazards to human health [15].

2.4 Numerical simulation method

To simulate current production situation, the geometric model consists of a tapping space and a dust collection hood. Physical model and mesh generation are shown in Figure 4.

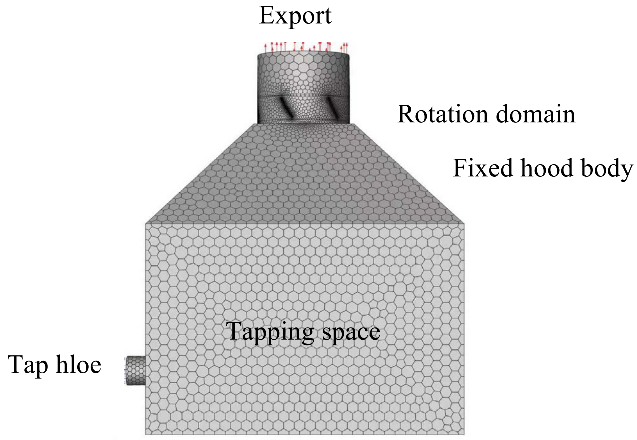

Fig.4. Physical model and mesh generation

The length and width of a tapping space are 3 meters, and the height is 2 meters. The height of a fixed hood body is 1 meter, and the height of a rotation domain is 0.25 meters. The top surface of a rotation domain is 0.4 meters away from the export. Diameter of a tap hole is 0.3m and the center of circle is 0.65m above ground. Mesh generation adopts Hex-Dominant unstructured mesh, rotation blades are locally densified, and a total mesh number is 517750. As mesh number continues to increase, airflow velocity on the tap hole center line has no significant change, so this mesh number is appropriate.

The flue gas is gas-solid two-phase flow which is composed of high-temperature gas and solid dust. The gas can be regarded as incompressible ideal gas. The k-ω SST model has strong applicability in complex flows and can more accurately simulate the flow characteristics within the boundary layer [16], so apply it to accurately simulate the flow field distribution inside. There is no chemical reaction during dust removal process, and dust volume fraction in the gas is less than 10%, therefore, a discrete phase model (DPM) is selected [17].

The boundary condition of inlet is set as a velocity inlet, and flow direction is perpendicular to the inlet cross-section. The boundary condition of outlet is set as a pressure outlet, and particles escape from it. All walls are immobile and conform to the no slip boundary condition. Coupled scheme is used to Pressure-velocity coupling, Least Squares Cell based is used to spatial discretization gradient, and second-order upwind scheme is used to obtain density, pressure, momentum, turbulent kinetic energy, and specific dissipation rate. Particle size distribution adopts Rosin-Rammler distribution and the drag criterion adopts the Stokes Cunningham model, Transient analysis is adopted with a time step of 0.01s. To verify the accuracy and reliability of this simulation, compare production site data with simulated data of airflow velocity on tap hole center line. The results are shown in Table 3. The airflow velocity at different locations on the production site are measured by hot-wire anemometers (FZ-4/5). The simulated data are calculated by Fluent, which based on the physical model and the determined numerical method established in the previous text. The velocity difference at different distances is not significant between two kinds of data, therefore, it can be considered that the simulation is accurate and reliable.

Table 3

The comparison results of airflow velocity on the taphole centerline

X(m)	X=0.5	X=1	X=1.5	X=2	X=2.5
Production site data (m/s)	23.45	20.12	15.78	10.69	7.73
Simulated data (m/s)	24.17	20.98.	16.45	11.94	8.38

Lagrangian method is used for solid phase. Trajectories of discrete phase particles are determined by integrating forces differential equations acting on particles [18]. In this paper, gravity force and dragging force of airflow on particles are considered, thermal radiation force and pressure gradient force are ignored [19,20]. equilibrium equation for the forces acting on particles is as follows:Initial velocity of flue gas jet is difficult to measure, but based on its generation characteristics, it can be determined using the formula for free outflow velocity through a small orifice [21].

$$V = \varphi\sqrt{\frac{2\Delta P}{\rho}} \tag{1}$$

φ is flow velocity coefficient with a value of 0.707; ΔP is pressure at the tap hole with a value of 1000Pa; ρ is density of dusty flue gas with a value of 1.5kg/m. According to the above formula, initial velocity of flue gas jet is calculated to be 25m/s.

3. Results

3.1 Flow field distribution

3.1.1 Flow field distribution of different rotation domain diameters

Rotation speed is 3000r/min, blades number is 6, rotation domain diameters are 1m, 1.5m, and 2m. The gas streamline diagram at 0.6s is shown in figure5. Rotation domain diameter is 1m (Fig.5a), the injected gas flows continuously along the length direction (x-direction) until it hits the wall. The airflow is forced to deflect along the wall and then flow in the opposite direction of the incoming jet, forming upper and lower reflux gas. This phenomenon indicates that the suction force of the rotating blades on the lower airflow is insufficient, retaining the inertia of the inlet jet. It extends horizontally for a long distance and gradually deflects upwards after reaching the wall, making it difficult to guide the dusty airflow to the outlet in a timely manner. Some dust is easily trapped in the lower chamber. Rotation domain diameter is 1.5m (Fig.5b), the injected gas starts flowing upwards at X=0.6m, forming two vortices on the left and right sides of chamber and vortex intensity on the left side is higher than that on the right side, exhibiting uneven airflow distribution and asymmetric turbulence characteristics. The airflow velocity in the top rotating blade area is 70-150m/s, which is a high-speed and low-pressure zone with the strongest suction effect. When streamline of the vortex extends to vicinity of outlet, the circulating airflow will be "cut off" by suction force at the upper part and attracted to the outlet. In addition, this asymmetry forms a low resistance short-circuit channel between the chamber and the outlet, and the dusty airflow does not need to remain in the chamber, but will directly rush towards the outlet along this channel to complete the escape. Rotation domain diameter is 2m (Fig.5c), the injected gas flows in a straight line for 0.4m, then deviates by 0.5m in the Z direction and continues to move forward, forming a large-scale spiral vortex that runs through the lower part of cavity. The remaining part of the airflow moves upward in a spiral shape. This is due to the increased turning radius of the outer edge of the impeller in the rotational domain, which forms a narrow slot throttling effect and interferes with main upward airflow channel of the chamber. The upward airflow is blocked and biased, and the airflow in the lower part of the chamber forms a low-speed stagnant vortex. The dust retention cannot be smoothly discharged upward, and the capture efficiency decreases.Through the streamline diagrams of different rotation domain diameters, it can be seen that the size of rotation domain has a significant impact on the airflow distribution. It can be preliminarily judged that 1.5 meters is the optimal rotational domain diameter for forming a reasonable upward suction flow field structure under this parameter setting.

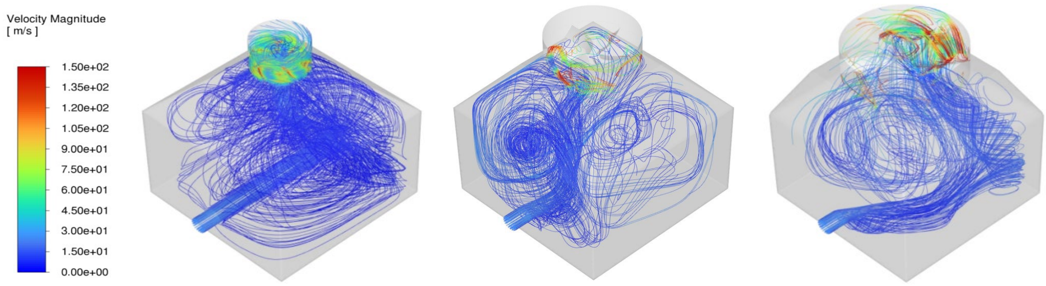

(a) 1 (b) 1.5 (c) 2m

Fig.5. The gas streamline diagram of different rotation domain diameters

3.1.2 Flow field distribution of different blades numbers

Rotation domain diameter is 1.5m, rotation speed is 3000r/min, blades number are 5, 6, 7. The gas streamline diagram at 0.6s is shown in figure6. The blades number is 5 (Fig.6a), the injected gas always flows in the x-direction until it hits the wall, and then undergoes strong deflection along the wall in the direction of the rotation domain. The streamlines intertwine and twist with each other, showing strong turbulent mixing characteristics. This indicates that the overall disturbance coverage of the airflow caused by rotation in the chamber is insufficient, and the active suction effect is difficult to extend to the lower iron outlet area, which cannot effectively guide the upward discharge of dusty airflow. The blades number is 6 (Fig.6b), injected gas flows out from the inlet and is quickly guided upward by the suction effect of the rotating blades. The suction channel is smooth, and the overall airflow flows upward in an orderly manner along the central area towards the outlet. The blades number is 7 (Fig.6c), the injected gas continues to flow in the x-direction until it hits the wall, and then the gas forms wall attached flow structure. This is because when blades number increases to 7, the spacing between blades decreases, and the airflow resistance in the rotating area increases significantly. Due to the blocking effect of the blades, the upward airflow is blocked, which is very unfavorable for the upward transportation of dusty airflow. Comparing the streamline distribution of three types of blade numbers, 6 blades can ensure sufficient rotational disturbance coverage without significant airflow blockage effects, and can form a upward flow field, which is the optimal number of blades under current parameters.

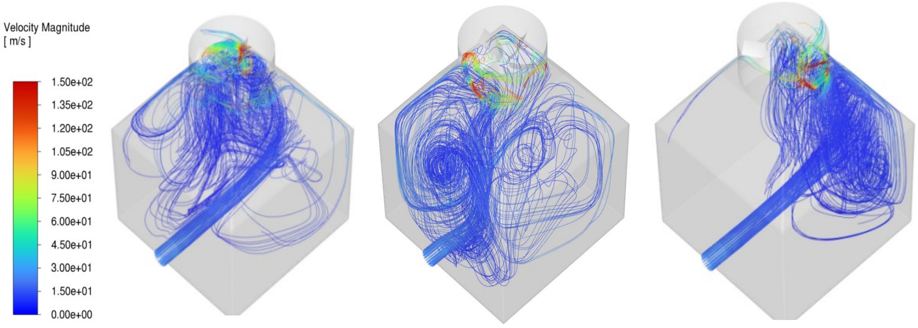

(a) 5 (b) 6 (c) 7

Fig.6. The gas streamline diagram of different blades number

3.1.3 Flow field distribution of different rotation speeds

Rotation domain diameter is 1.5m, blades number is 6, rotation speeds are 2000r/min, 3000r/min, 4000r/min. The gas streamline diagram at 0.6s is shown in figure7. Rotation speed is 2000r/min (Fig.7a), most of the airflow in the middle forms multiple small-scale vortices, and the circulating airflow cannot reach the outlet. A small portion of the airflow on both sides rises in a curved form to reach the outlet. It indicating that suction force of rotating blades on the lower airflow is insufficient at low speeds. Rotation speed is 3000 r/min (Fig.7b) , the airflow flowing out of the inlet is quickly guided upward by the rotating suction effect, forming a stable and smooth upward channel along the central area. Rotation speed is 4000r/min (Fig.7c), its gas flow line is similar to that of 3000 r/min, the middle airflow rises towards the outlet, and vortices appear on both sides. But, the flow line below the right vortex undergoes severe distortion and disorder, causing some airflow to be trapped in the lower part of chamber. Comparing the flow field structures under three different rotational speeds, it can be found that a rotation speed of 3000r/min can provide sufficient suction force to guide the upward flow of dusty air and is the optimal rotation speed under the current parameter settings.

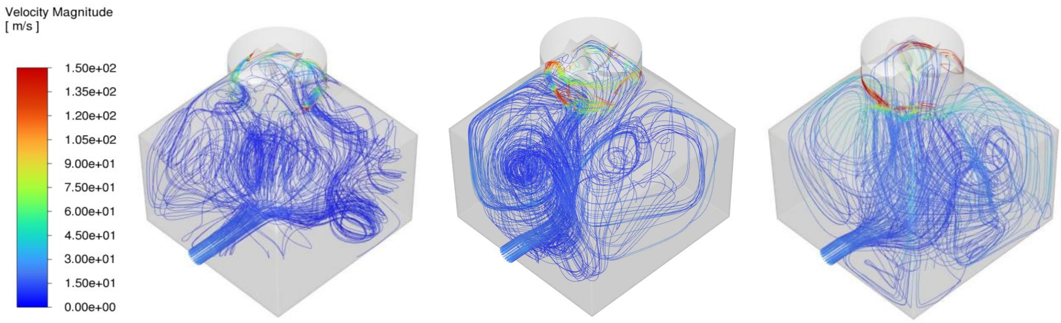

(a) 2000r/mi (b) 3000r/mi (c) 4000r/mi

Fig.7. The gas streamline diagram of different rotation speeds

3.2 Particle distribution

3.2.1 Particle distribution of different rotation domain diameters

Rotation speed is 3000r/min, blades number is 6, rotation domain diameters are 1m, 1.5m, and 2m. The particle distribution at 0.6s is shown in figure8. Rotation domain diameter is 1m (Fig.8a), particles are directly sprayed onto the opposite wall. Some particles move upwards along the wall, while others settle to the bottom and gather in the lower right corner. The rising particles reach the upper outlet at 1.8s. Rotation domain diameter is 1.5m (Fig.8b), particles begin to move upward along the middle channel near inlet (x=0.6m) and reach outlet at 0.6s, indicating that disturbance and suction ability of rotating blades are strongest at this time. Rotation domain diameter is 2m (Fig.8c), particles at inlet first settle downwards until they touch ground, then start moving upwards at x=1m and reach outlet in 0.8s. According to the particle distribution map, it can be seen that particle capture effect is best when rotation domain diameter is 1.5m. The results of these particle distributions are consistent with the previous gas flow field analysis, and also verify rationality of conclusions drawn from the previous flow field analysis.

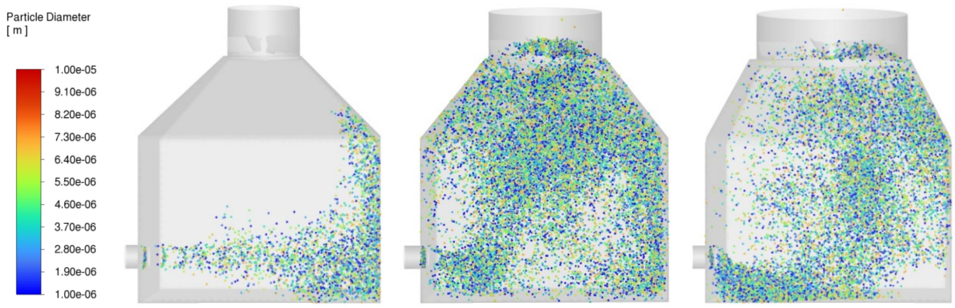

(a) 1m (b) 1.5m (c) 2m

Fig.8. The particle distribution of different rotation domain diameters

3.2.2 Particle distribution of different blades numbers

Rotation domain diameter is 1.5m, rotation speed is 3000r/min, blades number are 5, 6, 7. The particle distribution at 0.6s is shown in figure9. Blades number is 5 (Fig.9a), the particles are directly sprayed onto the wall. Most of particles settle in the lower right corner, with only a small amount of particles moving upwards, and finally reach the upper outlet at 1.8s. The situation where the blades number is 6 (Fig.9b) has been described in the previous section. Blades number is 7 (Fig.9c), the particles mainly move forward. After hitting the right wall, most of the particles settle to the lower right corner, with only a small amount of particles moving upward. And finally reach the upper outlet at 1.0s. Comparing the particle distribution under three different blade numbers, it can be found that when blade number is 5 or 7, most of the particles cannot move upward in time, and a large number of particles deposit and remain in the lower right corner of the cavity. The final time to reach the outlet is significantly longer, and the capture efficiency is low. Only when the number of leaves is 6, can the capture and discharge be completed in the shortest possible time, with almost no particles depositing in large quantities in the lower area of the cavity. Within this parameter range, 6 blades are the most suitable number of dust capture blades.

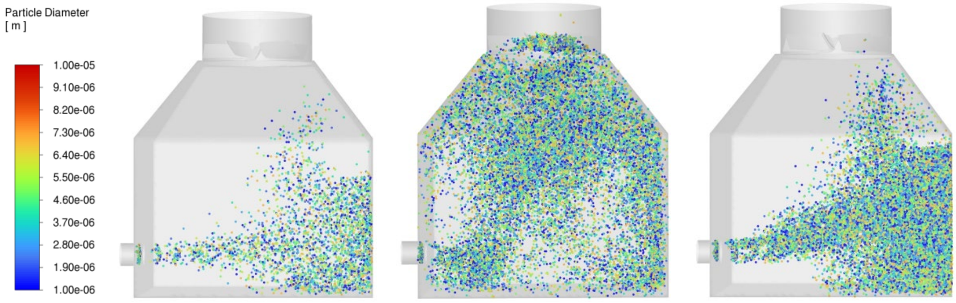

(a) 5 (b) 6 (c) 7

Fig.9. The particle distribution of different blades numbers

3.2.3 Particle distribution of different rotation speeds

Rotation domain diameter is 1.5m, blades number is 6, rotation speeds are 2000r/min, 3000r/min,4000r/min. The Particle distribution at 0.6s is shown in figure10. Rotation speed is 2000r/min (Fig.10a), the particles begin to settle downwards at x=1, pushing them forward on the ground and reaching the bottom right corner where they are squeezed and flow upwards. They reach the upper outlet at 1.4s. Rotation speeds is 4000r/min(Fig.10c), particles distribution is basically similar with 3000r/min, but there is more particles accumulation in the lower right corner at 4000r/min. Comparing the particle distribution results at three different speeds, it can be found that a speed of 3000r/min can maintain smooth upward movement of particles, minimize particle deposition, and achieve the best capture effect. This particle distribution is completely consistent with the flow field analysis results.

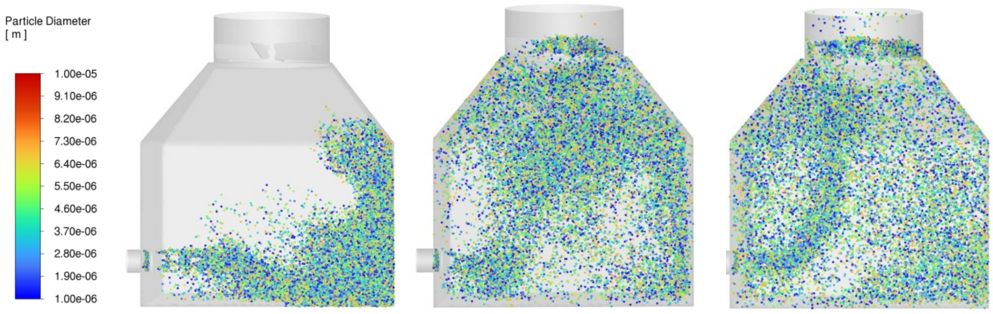

(a) 2000 r/min (b) 3000 r/min (c) 4000 r/min

Fig.10. The particle distribution of different rotation speeds

3.3 Capture efficiency of different conditions

Capture efficiency is the core indicator for evaluating dust collection hood performance. In this article, capture efficiency is equal to ratio of the number of particles at outlet to the number of particles at inlet. The capture efficiency under different rotation domain diameters and blade numbers with a constant rotation speed is shown in Figure 11 (a). As rotation domain diameter and blades number increase, the capture efficiency first increases and then decreases. When rotating domain diameter is 1.5 meters and blades number is 6, the capture efficiency reaches maximum; When rotation domain diameter is 1.5 meters and blades number is 6, the capture efficiency at different rotation speeds is shown in Figure 11 (b). As the rotation speed increases, the capture efficiency also first increases and then decreases. When the speed reaches 3000r/min, the capture efficiency reaches its peak.

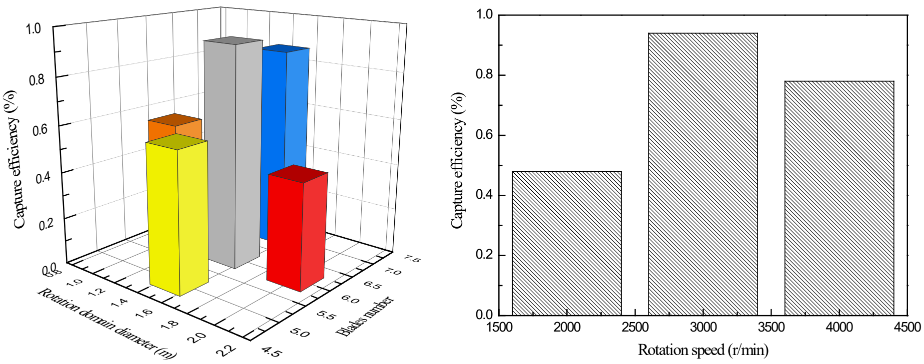

(a)Capture efficiency of different rotation domain diameters and blades numbers
(b) Capture efficiency of different rotation speeds
Fig.11. The capture efficiency of each operating condition

Pressure loss was measured as shown in Figure 12. Pressure loss increases with the increase of rotational domain diameter and rotational speed. The pressure losses are 295Pa and 390Pa under rotation domain diameter of 1m, rotation speed of 2000r/min. In these two operating conditions, the negative pressure in outlet area is lower and the suction force is weaker, making it difficult to fully suck dusty flue gas into dust collection hood, resulting in poor dust capture efficiency. When the rotation domain diameter increases to 2m and the rotation speed increases to 4000r/min, pressure loss increases significantly, energy consumption increases, and the flow field stability decreases, which is not conducive to stable flue gas capture and increases overall operating costs. The pressure loss is within a reasonable range under rotation domain diameter of 1.5m, 6 blades, and 3000r/min, taking into account both capture efficiency and operating energy consumption, making it a relatively optimal parameter combination.

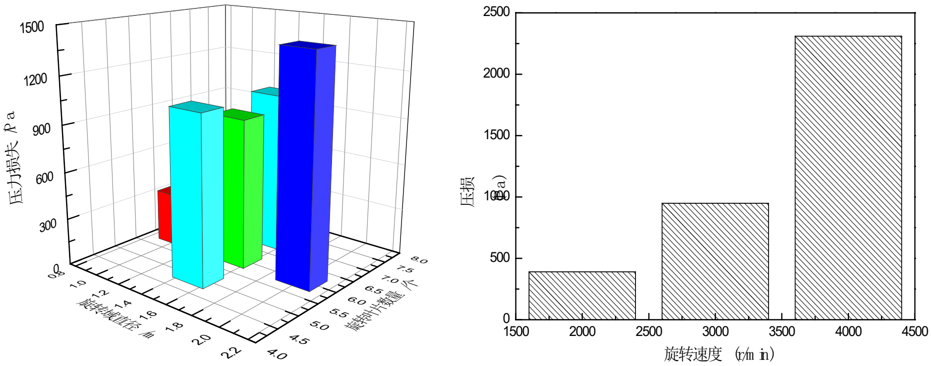

(a) Pressure loss of different rotation domain diameters and blades numbers
(b) Pressure loss of different rotation speeds
Fig.12. The capture efficiency of each operating condition

The optimal structure of dust collection hood was subjected to a industrial test in a certain steel enterprise. A dust sampling point that meets national standards is set up downstream of the dust hood exhaust outlet. A constant velocity sampler (Laoying 3012H) is used to collect dust samples, with a sampling flow rate controlled at 20L/min. Each sampling point is sampled continuously for no less than 30 minutes, three times a day, and the average value is taken as the daily dust concentration. The experimental results showed that after installing the new dust hood, the actual measured dust capture efficiency reached 92.3%, with an error of less than 2% compared to the 94% capture efficiency obtained from numerical simulation, verifying the reliability of the simulation results. The dust removal effect is shown in Figure 12.

Fig.12. The Dust removal effect on production site

3.4 Discussion

Wang[12] used the realizable k-ε model to simulate capture efficiency of traditional dust hoods at different positions. Lv[13] used the standard k-ε model to investigate capture efficiency with different opening angle of traditional dust hoods. Geng[14] used realizable k-ε model to simulate the effect of dust hood height and size on capture efficiency. The above research focuses on stable flow of airflow inside the fixed dust hood. This study addresses the pain points of weak suction, poor adaptability, and low particle capture efficiency of traditional fixed dust collection hoods at blast furnace tap holes. A top rotating blade type composite dust collection hood is proposed, and the SSTk-ω+DPM numerical simulation method is used to reveal the internal mechanism of enhanced dust removal by rotational disturbance from the two dimensions of gas flow field structure and particle capture. This provides theoretical basis and engineering reference for optimizing high-efficiency dust removal equipment at blast furnace tap holes. The active forced vortex generated by rotating blades and the superposition of negative pressure in the system are the core driving forces for reconstructing the flow field and improving dust control capabilities. In this study, the particle capture process is highly coupled with the flow field structure. The excellent flow field provides sufficient suction, stable upward channels, and low resistance paths. The particles change their inertial trajectory, shorten their residence time, and reduce bottom sedimentation under strong drag and vortex effects, achieving efficient capture. The active disturbance technology of rotating blades has broken through the efficiency bottleneck of traditional static dust removal hoods relying on passive negative pressure, and is more suitable for the complex working conditions of high temperature, high speed, and instantaneous high concentration at the tap holes of blast furnaces. The optimal matching relationship between rotation domain diameter, blades number , and rotation speed has been clarified, revealing the inherent mechanism of "vortex enhancement-flow field optimization-particle controllability-efficient capture", providing a quantitative basis for the design and operation of rotary dust removal equipment.

3.5 Limitations

This study is the first to apply the active disturbance technology of rotating blades to the dust removal of blast furnace tap holes, filling the research gap of dynamic dust removal technology in this field. However, there are still certain limitations in the research: firstly, the temperature changes throughout the blast furnace tapping process have not been considered; Secondly, long-term testing of high temperature resistance and wear resistance of blade materials has not been conducted, and the durability of industrial applications needs further verification; Thirdly, the energy consumption of the rotary drive system has not been finely optimized, and in the future, it can be further reduced by combining variable frequency control to lower operating costs.The exploration and resolution of these issues will help promote the wider industrial application of this technology and contribute to the clean production and sustainable development of the steel industry.

4. Conclusions

This article improves the traditional dust collection hood by setting up a rotation domain with blades on the upper part, using the SST k-ω turbulence model and DPM discrete element simulation technology to numerically simulate the airflow streamline distribution, particle distribution, and capture efficiency under different rotation domain diameters, blade numbers, and rotation speeds. Obtain the following conclusion: Airflow disturbance increases the suction force, and the magnitude of the suction force directly affects the movement trajectory of dust particles; Strong suction force can more effectively draw dust particles from the vicinity of the pollution source and promote them to move along a predetermined path towards the outlet, increasing the probability of particle capture; On the contrary, if the suction force is insufficient, dust particles may settle or diffuse due to their own gravity or other steady airflow, resulting in a decrease in capture efficiency; Under the optimal combination of structural parameters in this study, when the rotation domain diameter is 1.5 meters, blades number is 6, and rotation speed is 3000 r/min, the disturbance in the flow field is most sufficient and the suction force is most strong, resulting in the highest ratio of particle quantity at the outlet to the inlet, the peak capture efficiency reaches 94%, fully reflecting the important influence of fluid structure and particle dynamics on capture efficiency. This study has made significant progress in dust removal technology for blast furnace tap holes, but there is still space for further deepening and expansion in material reliability, energy consumption optimization, dust resource utilization. The exploration and resolution of these issues will help promote the wider industrial application of this technology and contribute to the clean production and sustainable development of the steel industry.

R E F E R E N C E S

[1]. *B. Rahmatmand, A. Tahmaseb, H. Lomas and T. Honeyandsl,* "A technical review on coke rate and quality in low-carbon blast furnace ironmaking"*,* in Fuel., **vol. 336**, Sept. 2023*, pp.* 127077

[2]. *Y. Xin, W. Li, J. Geng*, "Blast furnace iron mouth abnormalities and treatment", in Henan Metallurgy., **vol. 32**, no. 1, July. 2022, pp. 30-33

[3]. *Y. Owusu-Acheaw, M. Liu, G. Ma and X. Zhang,* "Recovery of Valuable Metals from Blast Furnace Dust by Iron-Bath Process", in Journal of Sustainable Metallurgy., **vol. 11**, Mar. 2025, pp. 1511-1524

[4]. *T. Rong, Y. Yuan, H. Yang and H. Yu*, "Investigation of the enrichment-purification process and electrochemical performance of kish graphite in dust from blast furnace tapping yard", in Waste Management., vol. **175**, Jan. 2024, pp. 121-132

[5]. *W. Nie, C. Jiang, Q. Liu and H. Wang*, "Study of dust pollution control effect based on orthogonal test and CFD numerical simulations", in Environmental Science and Pollution Research., **vol. 31**, Sept. 2024, pp. 43712-43730

[6]. *J. Mo, W. Ma*, "Researches on the numerical simulation of the dust pollution characteristics and the optimal dust suppression wind-speed on fully mechanised caving face", in Energy Exploration& Exploitation., **vol. 40**, no. 2, Mar. 2022, pp. 800-815

[7]. *P. Nirlipta, D. Nayak*, "Characterization of blast furnace flue dust- an assessment for its utilization", in Materials Today: Proceedings., **vol. 50**, Sept. 2022, pp. 2078-2083

[8]. *Z. Chi*, "Analysis and Application of Dust Removal on the Raw Material Ore Tank of Blast Furnace in Ironmaking Plant", in Environmental Engineering., **vol. 24**, no. 4, Aug. 2006, pp. 73-76

[9]. *C. Wu, S. Wang, C. Yang and E. Wang*, "Renovation of the fume hood type dedusting system for the ConsteelEAF at SISG", in Southern metals., **vol. 163**, no. 4, Aug. 2008, pp. 61-62

[10]. *C. Robert, E. LeRoy*, "Dust off Your Foundry's Silica Control Measures", in Modern Casting., **vol. 91**, no. 11, Nov. 2001, pp. 90-94

[11]. *R. Boudhan, A. Jouber, K.* Gueraoui *and S. Durecu*, "Pulse-Jet Bag Filter Performances for Treatment of Submicronic and Nanosized Particles from Waste Incineration", in Waste & Biomass Valorization., **vol. 9**, no. 5, Feb. 2018, pp. 731-737

[12]. *H. Wang, P. Zhang, F. Zhu and J. Zhuang*, "Simulation study on diffusion and collection characteristics of high temperature smoke and dust in blast furnace cast house", in Environmental Engineering., **vol. 38**, no. 11, Nov. 2020, pp. 123-129

[13]. *T. Lv, S. Che, C. Guo and X. Wang*, "Flow field simulation and structure optimization of confined hood at transshipment point of coal conveyor belt", in Chinese Journal of Environmental Engineering., **vol. 7**, no. 7, Jul. 2013, pp. 2667-2672

[14]. *X. Geng, J. Yan*, "Optimization of dust control measures in steelmaking electric furnace workshop based on FLUENT", in Journal of Safety Science and Technology., **vol. 17**, no. 9, Sept. 2021, pp. 163-168

[15]. *Y. Luo, S. Li, Z. Wu and C. He*, "Research on the influence of dust collection pipeline and vacuum hood structure on the dust removal effect of polishing workshops", in Journal of Cleaner Production., **vol. 532**, Sept. 2025, 146961

[16]. *J. Foroozesh, F. Parvaz, S. Hosseini and S. Namuye*, "Computational fluid dynamics study of the impact of surface roughness on cyclone performance and erosion", in Powder Technology., **vol. 389**, Sept. 2021, pp. 339-354

[17]. *M. El-Emam, L. Zhou, L. Bai*, "Modeling and Performance Analysis of Different Gas-Bioparticle Cyclone Separators: CFD-DEM Simulations", in Ind. Eng. Chem. Res., **vol. 62**, Jun. 2023, pp. 18552-18578

[18]. *Y. Yang, Z. Shen, J. Xu*, "Numerical Analysis of the Dust Control Performance of a Countercurrent Swirling Configuration in the Flash Ironmaking Reactor", in ISIJ International., **vol. 62**, no. 11, Sept. 2022, pp. 2225-2235

[19]. *S. Agrawal, J. Wong, J. Song and O. Mercan*, "Assessment of the aerodynamic performance of unconventional building shapes using 3D steady RANS with SST k-ω turbulence model", in J Wind Eng Ind Aerodyn., **vol. 225**, no. 7, Jul. 2022,104988

[20]. *K. Logachev, A. Ziganshin, O. Averkova*, "Simulations of dust dynamics around a cone hood in updraft conditions", in Journal of occupational and environmental hygiene., **vol. 15**, no. 10, Sept. 2018, pp. 207-220

[21]. *F. Parvaz, S. Hosseini, K. Elsayed*, "Numerical investigation of effects of inner cone on flow field, performance and erosion rate of cyclone separators", in Separation and Purification Technology., **vol. 201**, Jan. 201, pp. 223-237